Letter

Two rhombic ice phases from aqueous salt solutions under graphene confinement

Wei Du [1,2] Yangjie Wang,[1,4] Junwei Yang,[3] and Jige Chen [1,2,4,*]

[1]*Shanghai Institute of Applied Physics, Chinese Academy of Sciences, Shanghai 201800, China*

[2]*University of Chinese Academy of Sciences, Beijing 100049, China*

[3]*School of Arts and Sciences, Shanghai Dianji University, Shanghai 201306, China*

[4]*Shanghai Advanced Research Institute, Chinese Academy of Sciences, Shanghai 201210, China*

(Received 27 December 2023; accepted 3 May 2024; published 10 June 2024)

Water exhibits rich ice phases depending upon its respective formation conditions, and in particular, the two-dimensional ice with nonhexagonal symmetry adsorbed on solids relates to the exceptional arrangement of water molecules. Despite extensive reporting of two-dimensional ice on various solid surfaces, the geometry and thermodynamics of ice formation from an aqueous salt solution are still unknown. In this Letter, we show the formation of single- and two-phase mixed two-dimensional rhombic ice from aqueous salt solutions with different concentrations under strong compressed confinement of graphene at ambient temperature by using classical molecular dynamics simulations and first-principles calculations. The two rhombic ice phases exhibit identical geometry and thermodynamic properties, but different projections of the oxygen atoms against solid surface symmetry, where they relate to the stable and metastable arrangements of water molecules confined between two graphene layers. A single-phase rhombic ice would grow from the confined saturated aqueous solutions since the previously stable rhombic molecular arrangement becomes an unstable high-energy state by introducing salt ions nearby. Our result reveals different rhombic ice phases growing from pure water and aqueous solutions, highlighting the deciding role of salt ions in the ice formation process due to their common presence in liquids.

DOI: 10.1103/PhysRevE.109.L062103

Introduction. Ice is water frozen or compressed into a solid state with an ordered geometry, and various ice phases occur depending on their respective formation temperatures and pressures [1–15]. The most common ice phase, i.e., ice I_h, has a hexagonal crystalline structure due to the perfectly hydrogen-bonded packing of water molecules on lattice points in a two-dimensional hexagonal space lattice. Consistently, two-dimensional ice adsorbed on solid surfaces first tends to form in hexagonal arrays of water molecules that resemble the structure of naturally occurring ice crystal I_h [5,11–13,16–20]. Meanwhile, the exceptional nonhexagonal geometry of two-dimensional ice, such as square, pentagonal, heptagonal, and octagonal arrangements, represents the diverse water-solid binding energy on the hydrophilic surfaces against the intrinsic hydrogen bond interaction between water molecules [2,11,12,16–19,21–25]. To date, the formation of the two-dimensional ice has been both theoretically and experimentally confirmed, suggesting its ubiquitous role in many physical processes like surface wetting, antifreezing, adhesion, friction, and so on [5,13,20,21,26–31].

It is well known in the literature and our previous work that a hydration shell of water molecules arranges around salt ions in aqueous solutions [32–39] and it is strongly involved in the interlayer water-solid interactions and formation of hydrated structures on the solid surface [40–42]. The formation of two-dimensional ice at a solid surface is attributed to a simultaneous balance between both water-water and water-solid interactions that consequently causes structural variation by introducing salt ions nearby. However, in contrast to the extensive reporting of the structural diversity of two-dimensional ice adsorbed on different solid surfaces, the geometry and thermodynamics of two-dimensional ice formation from an aqueous salt solution are much less well understood. Recently, a peculiar square geometry of two-dimensional ice was proposed from water molecules confined between two graphene layers or confined in double-walled carbon nanotubes at ambient temperature [2,21–25]. The square ice represents an exceptional rearrangement of water molecules under strong confinement whose geometry is against the ordinary hexagonal hydrogen bonding preference of water molecules and also the hexagonal graphite surface symmetry. The experimental observation of square ice by transmission electron microscopy is under heavy debate due to the possible participating of some salt contaminant like NaCl in water [2,22]. It is thus a significant challenge to clarify the controversial role of salt ions for a fundamental understanding of two-dimensional ice formation.

In this Letter, we report a systematic study of the two-dimensional rhombic ice formation process from various aqueous solutions at ambient temperature under strong compressed graphene confinement by using classical molecular dynamics (MD) simulations and first-principles calculations. By applying continuous external compression, two rhombic ice phases simultaneously grow from a thin

*chenjg@sari.ac.cn

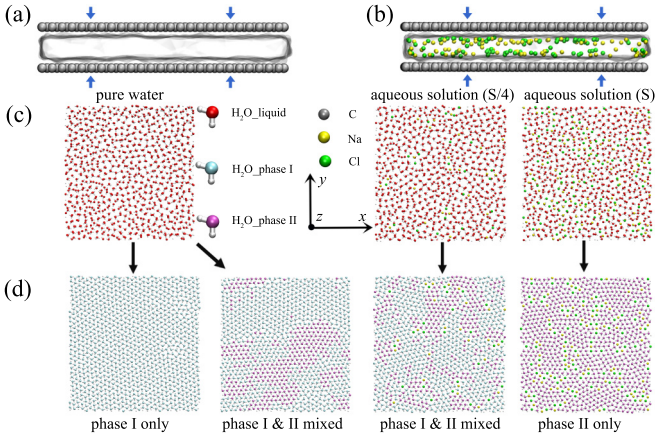

FIG. 1. Schematic of (a) the pure water layer and (b) the aqueous solution layer under compressed graphene confinement. The blue arrows indicate the external compression from the graphene layers. (c) Typical initial configurations of the thin pure water layer, the dilute NaCl solution layer (1/4 saturated concentration, denoted as $S/4$), and the saturated NaCl solution layer (denoted as S) before the external compression procedure. (d) Typical snapshots of the two-dimensional rhombic ice grown from the pure water and aqueous solutions. The two rhombic ice phases, phase I and II, possess different projections of oxygen atoms against surface symmetry and thus a clear boundary between each other. Oxygen atoms in water molecules in the initial liquid layer and the rhombic ice phases (I and II) are highlighted in red, blue, and purple.

layer of pure water or an aqueous solution between the graphene surfaces. The two ice phases possess identical geometry and thermodynamic properties like configuration entropy, tetrahedral order parameter, and hydrogen bond number, but with different projections of the oxygen atoms against solid surface symmetry. The two rhombic ice phases relate to the stable and metastable molecular arrangements by *ab initio* structure searching and density functional theory (DFT) calculations. A single rhombic ice phase grows in the saturated aqueous solutions since the previously stable arrangement of water molecules is an unstable high-energy state with the accompanying salt ions. Our finding enriches the two-dimensional ice phases under confinement and suggests a method to adjust ice phases with salt ions.

Methods. The schematics of the aqueous solutions under graphene confinement are shown in Figs. 1(a) and 1(b). The thin liquid layer, with a dimension of $61.4 \times 63.8 \times 6.4$ Å^3, is confined between two parallel graphene nanosheets. The zigzag direction of the graphene nanosheet is along the x axis and the armchair direction is along the y axis. The graphene nanosheet is rigid and the atomic bond length between the nonpolar carbon atoms is 1.42 Å. Periodic boundary conditions are applied in all directions. The particle-particle particle-mesh (PPPM) algorithm [43] is applied to solve the long-range Coulombic interactions and the height spacing of the simulation box is 80 Å to avoid artificial vertical interactions. The TIP4P/Ice water model [44] is used in the MD simulations performed by LAMMPS [45]. The Lennard-Jones parameters for atoms and ions are taken from those included in the OPLS-AA force field [46] and provided in PS1 in the Supplemental Material [47–56]. The concentration value of the NaCl solution ranges from 0 (pure water) to 5.4 mol/L (the saturated concentration value of the bulk solution, denoted as S) [57]. The classical MD simulations are performed in a NVT (canonical) ensemble at an ambient temperature 300 K in a Nosé-Hoover thermal bath. The simulations include two steps. (1) The equilibrium simulation is performed for the first 500 ps where the graphene nanosheets are fixed. (2) Next, the nonequilibrium simulation is performed for the next 600 ps by adding a constant opposite velocity 0.01 Å/ps to the top and bottom graphene nanosheets towards each other. The final distance between the two graphene nanosheets is 4.2 Å. A further compression about 0.1–0.7 Å would make the simulation system collapse. The analysis is thus performed before 1100 ps. For each simulation scenario, 12 ensemble averages, starting from different initial conditions, are considered to calculate the geometry and thermodynamic properties.

The first-principles calculations are performed in a much smaller system, as shown in Fig. 4. Two graphene nanosheets with 108 carbon atoms are kept at a distance 4.7 Å, which relates to the compressed distance of stable rhombic ice structures from the classical MD simulations. The graphene edges are passivated by H atoms to reduce the influence of unbonded edge electrons. A system of 14 water molecules refers to the pure water solution, while a system of ten water molecules, together with a Na^+ and a Cl^-, refers to the saturated solution. The *ab initio* structure searching is using the artificial bee colony algorithm in ABCluster and preoptimized by the semi-empirical tight-binding method [58,59]. Next, the DFT calculation is using the B3LYP-D3(BJ) method [60] with Becke-Johnson damping [61] to further optimize the stable structure and calculate its energy in GAUSSIAN 09 [62].

Results and discussion. The typical initial snapshots of liquid layers, i.e., the pure water, the dilute NaCl solution (1/4 saturated concentration, denoted as $S/4$), and the saturated NaCl solution (S) are illustrated in Fig. 1(c). By applying continuous compression through the moving graphene nanosheets, two-dimensional rhombic ice gradually grows from the confined aqueous solutions. Interestingly, it is found that the rhombic ice formation would be adjusted by the salt ions. The typical rhombic ice structures from the pure water and aqueous solutions are illustrated in Fig. 1(d) and their respective formation procedures over time are illustrated in PS2 in the Supplemental Material. As shown in Fig. 1(d), we observe two rhombic ice phases (phases I and II) from the confined pure water, growing in the form of either single-phase I or two-phase mixed (phases I and II mixed). The two ice phases exhibit the same geometry in the form of four water molecules arranged in a rhombic pattern, but with distinct projections of the oxygen atoms spreading on the graphene surface. As a result, a clear boundary is observed between the two ice phases. Similar two-phase mixed rhombic ices are growing in the dilute NaCl solution. By further increasing the concentration value, only the single-phase II rhombic ice is growing in the confined saturated NaCl solution.

To numerically demonstrate the geometry and thermodynamic properties of the two rhombic ice phases, we consider the configuration entropy S, tetrahedral order parameter M, and hydrogen bond number N_h of water molecules in the confined solutions as functions of time. The three quantities represent the structural variation of molecular configurations

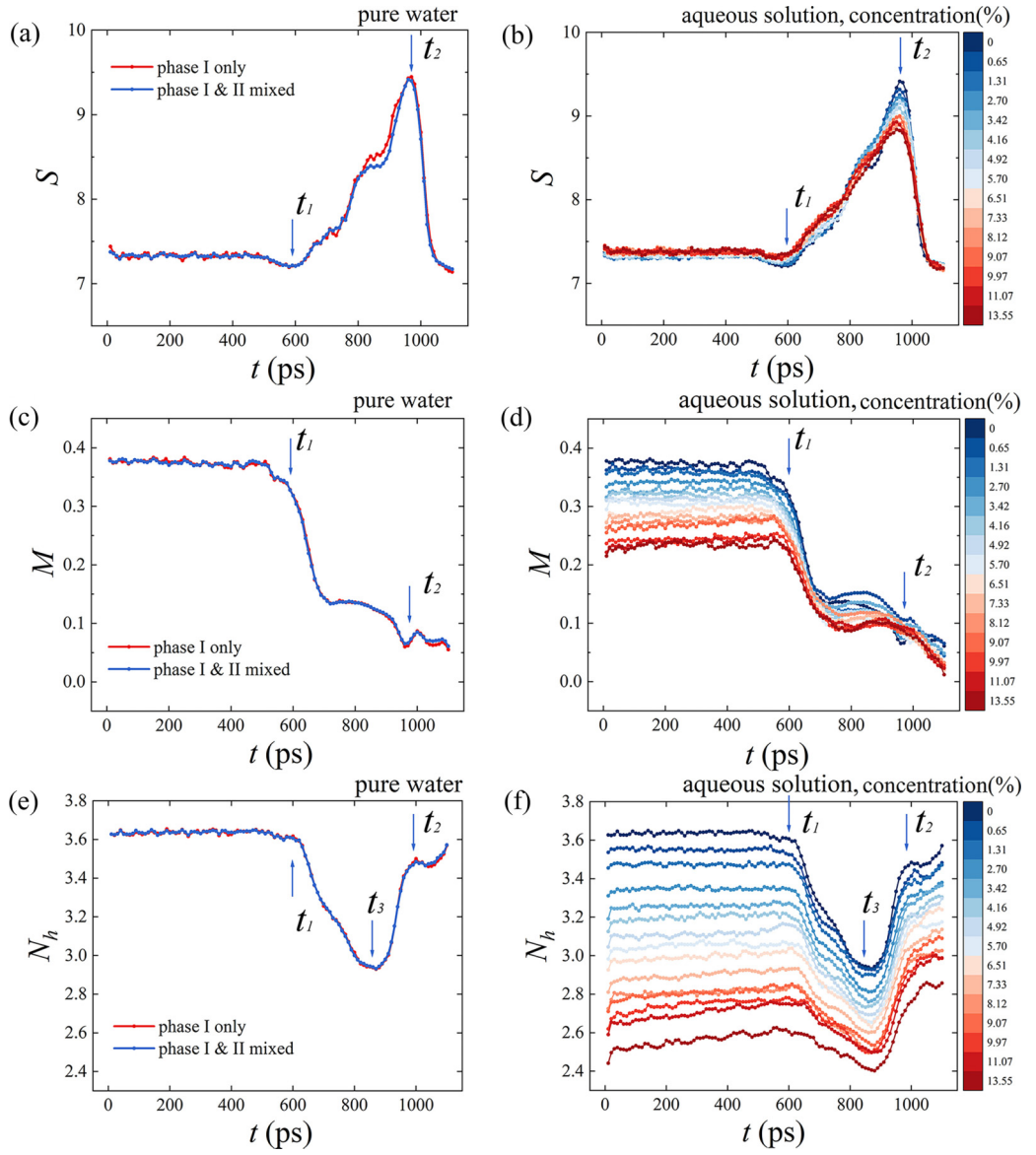

FIG. 2. (a) Configuration entropy S of the water molecules as a function of time, averaging over ensembles with formation of the rhombic ice in the pure water. S reaches its minimum value at t_1 and its maximum value at t_2. (b) Configuration entropy S in the NaCl solutions with different concentration values, ranging from pure water to saturated solutions. (c), (d) Tetrahedral order parameter M of the water molecules as a function of time in the (c) pure water and (d) NaCl solutions. (e), (f) The average hydrogen bond number N_h of the water molecules as a function of time in the (e) pure water and (f) NaCl solutions. N_h reaches its minimum value at t_3.

in the liquid layer during the compression procedure. The configuration entropy S is defined as follows [21,63,64]:

$$S = -k_B \sum_i \rho_\theta \ln\rho_\theta - k_B \sum_i \rho_\varphi \ln\rho_\varphi + S_r, \qquad (1)$$

where k_B is the Boltzmann constant and it is set to 1 for simplicity. θ, φ, and r are the three independent variables of the dipole moments of the water molecules in the spherical coordinate system (please see their schematic and time variations in PS3 in the Supplemental Material). θ and φ refer to the dipole orientation on the z axis and the orientation on the x axis in the x-y plane. ρ_θ and ρ_φ are their probability distributions. The distributions of θ and φ represent the planar and vertical degrees of freedom in the hydrogen network. They are regardless of molecule position of water molecules spreading on graphene surface. It provides a good measure of structural variations of the ice phases according to their hydrogen bond connections. Meanwhile, as a comparision, the configuration entropy of molecule position S_ψ is calculated in PS4 in the Supplemental Material. Its variation is two orders of magnitude smaller than the variation of S and thus not included in our entropy calculations. r refers to the magnitude of the dipole moments. r remains almost invariant and thus its entropy contribution $S_r = 0$. The tetrahedral order parameters M is defined as follows [1,21,65,66]:

$$M = 1 - \frac{3}{8} \sum_{j=1}^{3} \sum_{k=j+1}^{4} \left(\cos\alpha_{jk} + \frac{1}{3} \right)^2, \qquad (2)$$

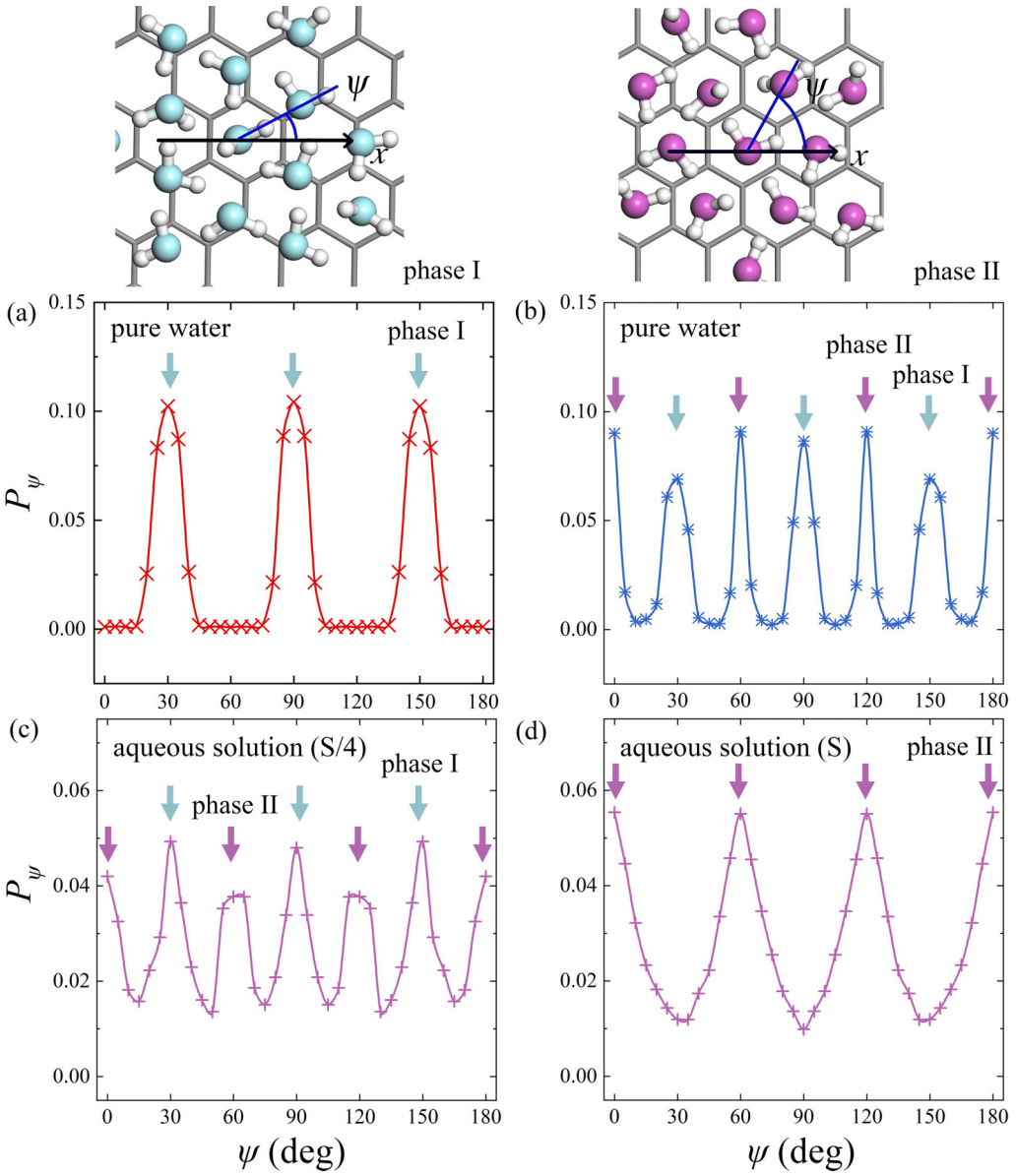

FIG. 3. Projection of the oxygen atoms ψ between two neighboring water molecules in the phase I and phase II rhombic ice. (a), (b) Probability distribution of ψ, P_ψ in the ensembles of the rhombic ice in (a) single-phase I and (b) two-phase mixed in the pure water. P_ψ in the ensembles of the rhombic ice in (c) two-phase mixed and (d) single-phase II in the dilute ($S/4$) and saturated (S) NaCl solutions.

where α_{jk} is the angle between a given water molecule' s oxygen atom and its two nearest-neighbors' oxygen atoms j, k. M is usually used to characterize the tetrahedral geometry of ice nucleation. Furthermore, the hexagonal order parameter h is calculated to characterize the hexagonal symmetry in PS5 in the Supplemental Material. Both the pure water and NaCl solutions exhibit an irregular increase of h in the compression process. The average hydrogen bond number N_h is calculated from the geometric criterion, i.e., $\theta_{\mathrm{OH-H}} \leqslant 30^\circ$ and $\mathrm{bond}_{\mathrm{O-O}} \leqslant 3.5$ Å. [1,21,67–69]. N_h is used to characterize the interaction strength between water molecules.

As shown in Figs. 2(a), 2(c) and 2(e), albeit with the final formation of either single-phase I or two-phase mixed rhombic ice, identical variations of S, M, and N_h in the compression procedure are obtained by calculating their respective ensemble averages in the confined pure water. Similarly, as shown in Figs. 2(b), 2(d) and 2(f), although with the final formation is either two-phase mixed or single-phase II rhombic ice, variations of S, M, and N_h are quite alike in the confined NaCl solutions with different concentration values. It implies that, without considering the position of water molecules spreading on graphene, the two rhombic ice phases are indistinguishable in geometry and thermodynamic properties during their formation procedures. Meanwhile, there are three characteristic times, t_1, t_2, and t_3, during the compression procedure. They are independent of the concentration value in the aqueous solutions and thus represent the intrinsic property of confined water. t_1 refers to the moment when the rhombic ice begins to grow in the liquid layer at 590 ps and S reaches its minimum value. It implies that the rhombic ice induces an entropy increase in the liquid layer. M and N_h exhibit a similar decrease starting from t_1, which

implies a deviation of the rhombic ice structure from the ordinary crystalline nucleation in ice I_h. t_2 refers to the moment when all the rhombic ice appears in the liquid layer at 960 ps and S reaches its maximum value. By further compressing the rhombic ice layer, the decreasing tendency of S implies a further ordering of the rhombic geometry. t_3 refers to the moment when N_h reaches its minimum value at 870 ps. It implies that a competition between the ordered and disordered arrangements breaks the hydrogen bonds during the rhombic ice formation. Furthermore, to numerically describe the compression strength, pressure variations in the liquid layer and S, M, and N_h as functions of pressure are illustrated in PS6 in the Supplemental Material.

To provide a quantitative description of the different spreading of water molecules on graphene surface in the two ice phases, we consider the projections of water molecules against the surface geometry of graphene. As shown in Fig. 3, a projection angle ψ is defined as the angle between the line connecting the oxygen atoms of two neighboring water molecules and the x axis from 0° to 180°. P_ψ is the probability distribution of ψ. For the single-phase I rhombic ice from the pure water, the peak values of P_ψ relate to ψ at 30°, 90°, and 150° in Fig. 3(a). For the single-phase II rhombic ice from the saturated NaCl, the peak values of P_ψ relate to ψ at 0°, 60°, and 120° in Fig. 3(d). It implies that the rhombic ice in phase II is a structure from a 30° rotation from the rhombic ice in phase I. It explains why the two rhombic ices are identical in geometry and thermodynamic properties, where they possess identical hydrogen bond connections. For the two-phase mixed rhombic ice from the pure water and dilute NaCl solutions, all six peaks of P_ψ are observed in Figs. 3(b) and 3(c). The time variations and full ensemble distributions of P_ψ are provided in PS7 in the Supplemental Material.

To understand the role of salt ions in the rhombic ice formation, we use *ab initio* structure searching to find the stable structure of confined water molecules. As shown in Fig. 4(a), the most stable structure relates to a rhombic arrangement in phase I and a metastable structure relates to a rhombic arrangement in phase II. The interaction energy difference between phase I and II structures is calculated to be $\Delta E = E_1 - E_2 = -3.37$ kCal/mol and -0.24 kCal/mol per water molecule. It is about one order of magnitude smaller than the energy of a hydrogen bond, which is -5.14 kCal/mol [70]. It explains the observation of the two-phase mixed rhombic ice since the energy difference between the two phases is negligible. However, only the rhombic arrangement in phase II is obtained in the *ab initio* structure searching by adding the Na^+ and Cl^- ions. We manually rotate the water molecules and salt ions by 30° to create the relative structure in phase I (please see the schematics in PS8 in the Supplemental Material). The phase I arrangement is now a high-energy state with accompanying salt ions. The interaction energy difference between phases I and II structures is calculated to be $\Delta E = E_1 - E_2 = 35.55$ kCal/mol and 3.56 kCal/mol per water molecule. It explains why only the single-phase II rhombic ice is obtained in the saturated NaCl solution. In addition, by increasing the simulation temperature up to 360 K, only phase I is growing in the pure water. It gives us the upper limit of the free-energy barrier from phases II to I

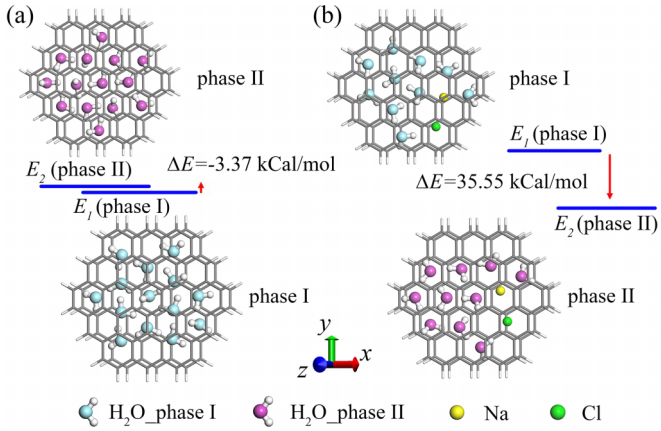

FIG. 4. (a) The most stable optimized structure and its interaction energy E_1 (phase I), together with the metastable optimized structure and its interaction energy E_2 (phase II), of confined water molecules between graphene nanosheets. Energy difference $\Delta E = E_1 - E_2$ is calculated. (b) The most stable optimized structure and its interaction energy E_2 (phase II) of confined water by adding the Na^+ and Cl^- ions. The interaction energy E_1 (phase I) is obtained by rotating the solution elements by 30° relative to the graphene nanosheets.

to be 0.04 kCal/mol per water molecule. Please see details in PS9 in the Supplemental Material.

Moreover, the rhombic ice formation is a general phenomenon in aqueous solutions. We choose the confined saturated LiCl, KCl, $CaCl_2$, $MgCl_2$, and $AlCl_3$ solutions with different cation types and valences as typical examples. Rhombic ice in single-phase II is observed with similar variations of S, M, and N_h. The same order of magnitude of interaction energy difference ΔE between phases I and II is obtained. Please see details in PS10 in the Supplemental Material.

Conclusion. In summary, we find two two-dimensional rhombic ice phases in the aqueous solutions under strong confinement of graphene at ambient temperature by using classicalMD simulations and first-principles calculations. The rhombic ices are indistinguishable in geometry and thermodynamic properties, but with distinct projections of the oxygen atoms against graphene surface symmetry. They relate to the stable and a metastable structures of confined water molecules. Only one rhombic ice phase remains in the confined saturated solutions since the other one becomes an unstable high-energy state with the accompanying salt ions. The result indicates salt ions heavily contribute to ice formation and enlightens our understanding of the complex water-solid-ion interactions in aqueous solutions.

Acknowledgments. This work was supported by the Natural Science Foundation of Shanghai (Grants No. 14ZR1448100 and No. 19ZR1463200), the International Partnership Program of the Chinese Academy of Sciences (Grant No. 307GJHZ2022065FN), the Academic Discipline Project of Shanghai Dianji University (Grant No. 16JCXK02), and the Postdoctoral Fellowship Program of CPSF (Grant No. GZC20231365). The authors thank the Big Data Science Center of Shanghai Synchrotron Radiation Facility, the Shanghai Supercomputer Center, and the Supercomputing Center of Chinese Academy of Sciences.

[1] A. Ben-Naim, *Molecular Theory of Water and Aqueous Solutions-Part 1: Understanding Water* (World Scientific, Singapore, 2009).

[2] G. Algara-Siller, O. Lehtinen, F. C. Wang, R. R. Nair, U. Kaiser, H. A. Wu, A. K. Geim, and I. V. Grigorieva, Nature (London) **519**, 443 (2015).

[3] A. Verdaguer, G. M. Sacha, H. Bluhm, and M. Salmeron, Chem. Rev. **106**, 1478 (2006).

[4] Y. Zheng, C. Su, J. Lu, and K. P. Loh, Angew. Chem. Int. Ed. **52**, 8708 (2013).

[5] R. Ma *et al.*, Nature (London) **577**, 60 (2020).

[6] G. A. Kimmel, J. Matthiesen, M. Baer, C. J. Mundy, N. G. Petrik, R. S. Smith, Z. Dohnalek, and B. D. Kay, J. Am. Chem. Soc. **131**, 12838 (2009).

[7] S. Maier, B. A. J. Lechner, G. A. Somorjai, and M. Salmeron, J. Am. Chem. Soc. **138**, 3145 (2016).

[8] K. Xu, P. Cao, and J. R. Heath, Science **329**, 1188 (2010).

[9] K. T. He, J. D. Wood, G. P. Doidge, E. Pop, and J. W. Lyding, Nano Lett. **12**, 2665 (2012).

[10] D.-S. Yang and A. H. Zewail, Proc. Natl. Acad. Sci. **106**, 4122 (2009).

[11] J. Chen, G. Schusteritsch, C. J. Pickard, C. G. Salzmann, and A. Michaelides, Phys. Rev. Lett. **116**, 025501 (2016).

[12] X. Zhang *et al.*, Phys. Rev. Lett. **121**, 256001 (2018).

[13] C. Zhu, Y. Gao, W. Zhu, J. Jiang, J. Liu, J. Wang, J. S. Francisco, and X. C. Zeng, Proc. Natl. Acad. Sci. **116**, 16723 (2019).

[14] R. Sutcliffe and J. G. Rau, Phys. Rev. B **105**, 104405 (2022).

[15] H.-T. Chin *et al.*, Nat. Commun. **12**, 6291 (2021).

[16] J. Carrasco, A. Michaelides, M. Forster, S. Haq, R. Raval, and A. Hodgson, Nat. Mater. **8**, 427 (2009).

[17] S. Nie, P. J. Feibelman, N. C. Bartelt, and K. Thurmer, Phys. Rev. Lett. **105**, 026102 (2010).

[18] A. Shiotari and Y. Sugimoto, Nat. Commun. **8**, 14313 (2017).

[19] C. Lin, N. Avidor, G. Corem, O. Godsi, G. Alexandrowicz, G. R. Darling, and A. Hodgson, Phys. Rev. Lett. **120**, 076101 (2018).

[20] P. Yang, C. Zhang, W. Sun, J. Dong, D. Cao, J. Guo, and Y. Jiang, Phys. Rev. Lett. **129**, 046001 (2022).

[21] Y. Wang and J. Chen, J. Stat. Mech. (2023) 063203.

[22] W. Zhou *et al.*, Nature (London) **528**, E1 (2015).

[23] B. Lin, J. Jiang, X. C. Zeng, and L. Li, Nat. Commun. **14**, 4110 (2023).

[24] Z. Qiao, Y. Zhao, and Y. Q. Gao, J. Phys. Chem. Lett. **10**, 3115 (2019).

[25] Y. Liu, J. Jiang, Y. Pu, J. S. Francisco, and X. C. Zeng, ACS Nano **17**, 6922 (2023).

[26] K. Liu, C. Wang, J. Ma, G. Shi, X. Yao, H. Fang, Y. Song, and J. Wang, Proc. Natl. Acad. Sci. **113**, 14739 (2016).

[27] J. Liu, C. Zhu, K. Liu, Y. Jiang, Y. Song, J. S. Francisco, X. C. Zeng, and J. Wang, Proc. Natl. Acad. Sci. **114**, 11285 (2017).

[28] L. Chen and L. Qian, Friction **9**, 1 (2021).

[29] B. Radha *et al.*, Nature (London) **538**, 222 (2016).

[30] S. Han, M. Y. Choi, P. Kumar, and H. E. Stanley, Nat. Phys. **6**, 685 (2010).

[31] V. Kapil, C. Schran, A. Zen, J. Chen, C. J. Pickard, and A. Michaelides, Nature (London) **609**, 512 (2022).

[32] H. Ohtaki and T. Radnai, Chem. Rev. **93**, 1157 (1993).

[33] J. Mähler and I. Persson, Inorg. Chem. **51**, 425 (2012).

[34] R. Pérez de Tudela and D. Marx, Phys. Rev. Lett. **119**, 223001 (2017).

[35] W. Fan, J. Chen, X. Lei, and H. Fang, Phys. Chem. Chem. Phys. **19**, 30055 (2017).

[36] A. C. LaForge, R. Michiels, M. Bohlen, C. Callegari, A. Clark, A. von Conta, M. Coreno, M. Di Fraia, M. Drabbels, M. Huppert, P. Finetti, J. Ma, M. Mudrich, V. Oliver, O. Plekan, K. C. Prince, M. Shcherbinin, S. Stranges, V. Svoboda, H. J. Worner, and F. Stienkemeier, Phys. Rev. Lett. **122**, 133001 (2019).

[37] L. Mu, Y. Yang, J. Liu, W. Du, J. Chen, G. Shi, and H. Fang, Phys. Chem. Chem. Phys. **23**, 14662 (2021).

[38] J. Yang, J. Chen, and H. Fang, Mol. Phys. **119**, e1919773 (2021).

[39] W. Du, J. Yang, J. Chen, and H. Fang, Mol. Phys. **120**, e2092040 (2022).

[40] J. Liu, G. Shi, P. Guo, J. Yang, and H. Fang, Phys. Rev. Lett. **115**, 164502 (2015).

[41] L. Chen *et al.*, Nature (London) **550**, 380 (2017).

[42] Y. Wang and J. Chen, Europhys. Lett. **139**, 51002 (2022).

[43] R. W. Hockney and J. W. Eastwood, *Computer Simulation Using Particles* (CRC Press, Boca Raton, FL, 1988).

[44] J. L. F. Abascal, E. Sanz, R. Garcia Fernandez, and C. Vega, J. Chem. Phys. **122**, 234511 (2005).

[45] S. Plimpton, J. Comput. Phys. **117**, 1 (1995).

[46] W. L. Jorgensen, D. S. Maxwell, and J. Tirado-Rives, J. Am. Chem. Soc. **118**, 11225 (1996).

[47] See Supplemental Material at http://link.aps.org/supplemental/10.1103/PhysRevE.109.L062103 for more details, which includes Refs. [48–56].

[48] D. R. Nelson and B. I. Halperin, Phys. Rev. B **19**, 2457 (1979).

[49] A. C. Mitus and A. Z. Patashinskii, Phys. Lett. A **98**, 31 (1983).

[50] R. Cohen *et al.*, Nat. Commun. **11**, 5137 (2020).

[51] J. E. McDonald, Am. J. Phys. **31**, 31 (1963).

[52] G. S. Redner, C. G. Wagner, A. Baskaran, and M. F. Hagan, Phys. Rev. Lett. **117**, 148002 (2016).

[53] A. C. Newell, T. Passot, and J. Lega, Annu. Rev. Fluid Mech. **25**, 399 (1993).

[54] X.-M. Bai and M. Li, J. Chem. Phys. **124**, 124707 (2006).

[55] V. I. Kalikmanov, in *Nucleation Theory* (Springer, Dordrecht, The Netherlands, 2013), p. 17.

[56] P. G. Vekilov, Cryst. Growth Des. **10**, 5007 (2010).

[57] T. Driesner and C. A. Heinrich, Geochim. Cosmochim. Acta **71**, 4880 (2007).

[58] J. Zhang and M. Dolg, Phys. Chem. Chem. Phys. **17**, 24173 (2015).

[59] J. Zhang and M. Dolg, Phys. Chem. Chem. Phys. **18**, 3003 (2016).

[60] S. Grimme, S. Ehrlich, and L. Goerigk, J. Comput. Chem. **32**, 1456 (2011).

[61] A. D. Becke and E. R. Johnson, J. Chem. Phys. **123**, 154101 (2005).

[62] M. J. Frisch *et al.*, GAUSSIAN 09, Rev D.01, 2009.

[63] L. D. Landau and E. M. Lifshitz, *Statistical Physics* (Third Edition) (Butterworth-Heinemann, Oxford, 1980).

[64] L. E. Reichl, *A Modern Course in Statistical Physics: Complexity and Entropy* (Wiley-VCH, Weinheim, Germany, 2016).

[65] J. R. Errington and P. G. Debenedetti, Nature (London) **409**, 318 (2001).

[66] C. Zhang and G. Galli, J. Chem. Phys. **141**, 084504 (2014).
[67] R. Zhang, G. Du, M. Wang, W. Yu, and J. Chen, J. Stat. Mech. (2019) 063210.
[68] Y. Lu, Y. Wang, and J. Chen, J. Stat. Mech. (2021) 053204.
[69] W. Fan and J. Chen, Phys. Rev. E **101**, 010101(R) (2020).
[70] K. Wendler, J. Thar, S. Zahn, and B. Kirchner, J. Phys. Chem. A **114**, 9529 (2010).